Exploring the intrinsic limit of the charge-carrier-induced increase of the Curie temperature of Lu- and La-doped EuO thin films

R. Held,[1] T. Mairoser,[2] A. Melville,[1] J. A. Mundy,[3] M. E. Holtz,[3] D. Hodash,[1] Z. Wang,[1] J. T. Heron,[1] S. T. Dacek,[1] B. Holländer,[4] D. A. Muller,[3,5] and D. G. Schlom[1,5,6]

[1]Department of Materials Science and Engineering, Cornell University, Ithaca, New York 14853, USA
[2]Zentrum für Elektronische Korrelationen und Magnetismus, Universität Augsburg, Universitätsstraße 1, D-86159 Augsburg, Germany
[3]School of Applied and Engineering Physics, Cornell University, Ithaca, New York 14853, USA
[4]Peter Grünberg Institut, Forschungszentrum Jülich, D-52425 Jülich, Germany
[5]Kavli Institute at Cornell for Nanoscale Science, Ithaca, New York 14853, USA
[6]Leibniz-Institut für Kristallzüchtung, Max-Born-Str. 2, 12489 Berlin, Germany

(Received 20 June 2020; accepted 28 September 2020; published 20 October 2020)

Raising the Curie temperature T_C of the highly spin-polarized semiconductor EuO by doping it with rare-earth elements is a strategy to make EuO more technologically relevant to spintronics. The increase of T_C with free carrier density n and the surprisingly low dopant activation p, found in Gd-doped EuO thin films [Mairoser *et al.*, Phys. Rev. Lett. **105**, 257206 (2010)], raised the important question of whether T_C could be considerably enhanced by increasing p. Using a low-temperature growth method for depositing high-quality Lu-doped EuO films we attain high dopant activation (p) values of up to 67%, effectively more than doubling p as compared to adsorption-controlled growth of Lu- and Gd-doped EuO. Relating n, p, and lattice compression of La- and Lu-doped EuO films grown at different temperatures to the T_C of these samples allows us to identify several different mechanisms influencing T_C and causing an experimental maximum in T_C. In addition, scanning transmission electron microscopy in combination with electron energy loss spectroscopy measurements on La-doped EuO indicate that extensive dopant clustering is one, but not the sole reason for dopant deactivation in rare-earth doped EuO films.

DOI: 10.1103/PhysRevMaterials.4.104412

I. INTRODUCTION

Many of the remarkable properties of the semiconductor EuO, including strong ferromagnetism, large Faraday rotation, and a giant insulator-to-metal transition, were discovered more than 40 years ago [1–4]. More recent work on thin films has demonstrated >90% spin polarization of electrical currents in doped EuO and the successful epitaxial integration of EuO with silicon, GaAs, and GaN [5–7]. The increasing structural perfection of EuO films grown directly on silicon may allow fabricating efficient spin filter contacts to silicon providing an alternative route for integrating spin filter functionality into silicon [8–10]. These qualities render EuO an outstanding material for spintronic studies and proof-of-concept devices. Furthermore, deposition of the easily overoxidized half-metallic semiconductor EuO does not always require expensive ultrahigh-vacuum equipment: By employing topotactic transformation EuO thin films with excellent quality can be fabricated using just high-vacuum means [11].

Stoichiometric EuO has a Curie temperature (T_C) of 69 K [12], which is comparable to the Curie temperatures of other spintronic materials like standard dilute semiconductor systems, such as manganese-doped GaAs, and well below the T_C values needed for commercial devices, but by doping EuO with oxygen vacancies (EuO_{1-x}) [4] or with rare-earth atoms such as gadolinium, lanthanum, lutetium, and scandium [13–18], the Curie temperature can be considerably enhanced. In addition, compressive epitaxial strain is expected to further increase T_C [19,20].

Below T_C, charge carrier transfer occurs in EuO from the donor level into the lower part of the Zeeman-split spin-polarized EuO 5d-6s conduction band [5]. One of the mechanisms responsible for the T_C increase by doping is the enhancement of the indirect exchange between the ferromagnetically ordered Eu 4f moments mediated by these additional free charge carriers up to a critical carrier density n_C. According to theoretical models describing this scenario, carrier densities beyond n_C lead to magnetic instabilities [21] or antiferromagnetic ordering [19] and to a T_C reduction.

Importantly, not all dopant atoms contribute an electron to the conduction band. The only published measurements quantifying the relationship between the doping concentration x and free carrier density n (allowing calculation of the fractions of active and inactive dopants), and T_C of doped EuO, are on Gd-doped EuO films [22–24]. These experiments show a roughly logarithmic increase of T_C up to 129 K when plotted as a function of n. For high doping concentrations $x \gtrsim 10\%$ the mobile carrier density saturates around

Published by the American Physical Society under the terms of the Creative Commons Attribution 4.0 International license. Further distribution of this work must maintain attribution to the author(s) and the published article's title, journal citation, and DOI.

1×10^{21} cm^{-3}. But most importantly, these measurements reveal a surprisingly low Gd dopant activation p of less than 35% for all films. Later, it was shown that T_C and p in Gd-doped EuO decrease strongly with increasing deposition temperature above $T \sim 350\,^{\circ}$C [24]. Interestingly, all of the samples in these works show high structural quality in either low-energy electron diffraction or x-ray diffraction (XRD) measurements with narrow rocking curve full width at half maximum (FWHM) values around 0.01° and no indications of possible structural changes of the films caused by Gd doping.

These prior findings raise several questions the answers of which could have tremendous implications on potential applications of EuO. First, which mechanisms are responsible for the deactivation of dopant carriers in EuO? Second, is it possible to increase the dopant activation and Curie temperature by optimizing the growth conditions or by using different dopants? Third, what are the experimental limits to the Curie temperature given by the various doping methods and strain?

Using a low-temperature, close to flux-matched growth method, we reach higher dopant activations and higher carrier densities than prior studies in Lu-doped EuO thin films, effectively tripling these values in samples with high T_C as compared to samples grown using standard adsorption-controlled growth. By comparing n, p, and T_C of La- and Lu-doped EuO films grown at different temperatures, we show that increasing n beyond $\sim 2 - 4 \times 10^{20}$ cm^{-3} has only a very limited effect on T_C in these samples. We find indications that at these high carrier densities, the maximum T_C of La- and Lu-doped samples is instead determined by a superposition of effects from dopant ion size, concomitant lattice compression, and reduced direct exchange caused by high doping concentrations of nonmagnetic ions. This is corroborated by x-ray diffraction and STEM-EELS measurements of La-doped EuO films that also rule out extended crystallographic defects as reason for the limited T_C of these films.

II. METHODS

To perform these experiments we deposited single-crystalline epitaxial La- and Lu-doped EuO thin films on (110) $YAlO_3$ and (110) $LuAlO_3$ substrates by reactive oxide molecular-beam epitaxy using two different growth techniques: standard adsorption-controlled growth and lower-temperature, close to flux-matched deposition. The thickness of the films was chosen to be ~ 35 nm, which is sufficiently thin to avoid structural relaxation of the EuO films grown on the $YAlO_3$ and $LuAlO_3$ substrates [20,25]. To dope the EuO films, we evaporated Eu and the dopant element at the same time from separate effusion cells at the desired ratio using a quartz crystal microbalance to calibrate the fluxes of the separate molecular beams. After growth, we capped the samples *in situ* with 50 nm of amorphous $LaAlO_3$ or 30 nm of amorphous silicon to protect them from further oxidation when exposed to air. We investigated the crystalline quality of almost all of the 42 films that are the subject of this study by four-circle x-ray diffraction.

It is challenging to grow stoichiometric EuO thin films, mainly because of their tendency to form higher oxides such as Eu_3O_4 and Eu_2O_3. This problem could be solved for many applications by using adsorption-controlled growth at substrate temperatures $>400\,^{\circ}$C. Previous work showed that using this method it is possible to reproducibly grow close-to-stoichiometric EuO films with excellent crystalline quality according to XRD [20,23–26]. Reaching a similar film quality with lower-temperature growth is much more challenging.

At the lower substrate temperatures of $T = 250\,^{\circ}\mathrm{C} - 275\,^{\circ}\mathrm{C}$ used for deposition of the close to flux-matched films in this study, almost all of the impinging Eu atoms stick to the growing film surface. This leads to a considerably smaller growth window for stoichiometric EuO as compared to growth at higher substrate temperature. As oxygen vacancies in EuO are expected to increase n and can also lead to a considerable T_C increase, [4,18] it is imperative to avoid these defects to be able to determine the intrinsic effect of rare-earth doping. On the other hand, oxygen-rich deposition conditions that lead to the formation of Eu_3O_4 or Eu_2O_3 are expected to reduce n and T_C. We overcame these conflicting issues by precisely mapping the growth window as a function of substrate temperature and oxygen partial pressure and meticulous calibration of the deposition conditions utilizing a residual gas analyzer (RGA) for accurate control of the relative oxygen partial pressure and reflection high-energy electron diffraction (RHEED) for *in situ* quality control. More details on film growth methods can be found in the Supplemental Material [27]. The adsorption-controlled samples were grown at $T = 400\,^{\circ}$C according to the recipe described elsewhere [24–26].

The T_C of the films was determined using superconducting quantum interference device (SQUID) magnetometry or vibrating sample magnetometry (VSM) following Ref. [28]. Measured magnetization characteristics are consistent with corresponding curves found in the literature (see Supplemental Material [27]). We determined the in-plane saturation magnetization (M_{sat}) and field (H_{sat}) from hysteresis loops measured at 5 K.

We measured the Hall resistance R_H at $T = 5$ K using $\sim$100-μm-wide Hall bars patterned by photolithography in combination with *in situ* ion etching and sputter deposition following the procedure described in Ref. [22] (see Supplemental Material [27]). These Hall effect measurements were used to determine the mobile charge carrier density n in the La- and Lu-doped EuO films. The ratio of n to the concentration of rare-earth dopants determined p, the dopant activation.

III. RESULTS

Figure 1(a) compares T_C and n of Lu-doped EuO films grown using adsorption-controlled or close to flux-matched conditions on $LuAlO_3$. It is evident that the samples deposited with both techniques reach comparable maximum T_C values around 126 K, but the Lu-doped samples grown at lower T exhibit much higher maximum mobile carrier densities as compared to their counterparts grown by adsorption control. The samples grown at $T = 250\,^{\circ}$C reach carrier densities of $\sim 1.6 \times 10^{21}$ cm^{-3} at 8%–12% doping concentration, which is 3.4 times the maximum value of the samples grown at $T = 400\,^{\circ}$C. This difference also manifests in the dopant activation [Fig. 1(b)]. While the Lu-doped samples grown at $T = 400\,^{\circ}$C exhibit activation levels below 33%, the Lu-doped samples

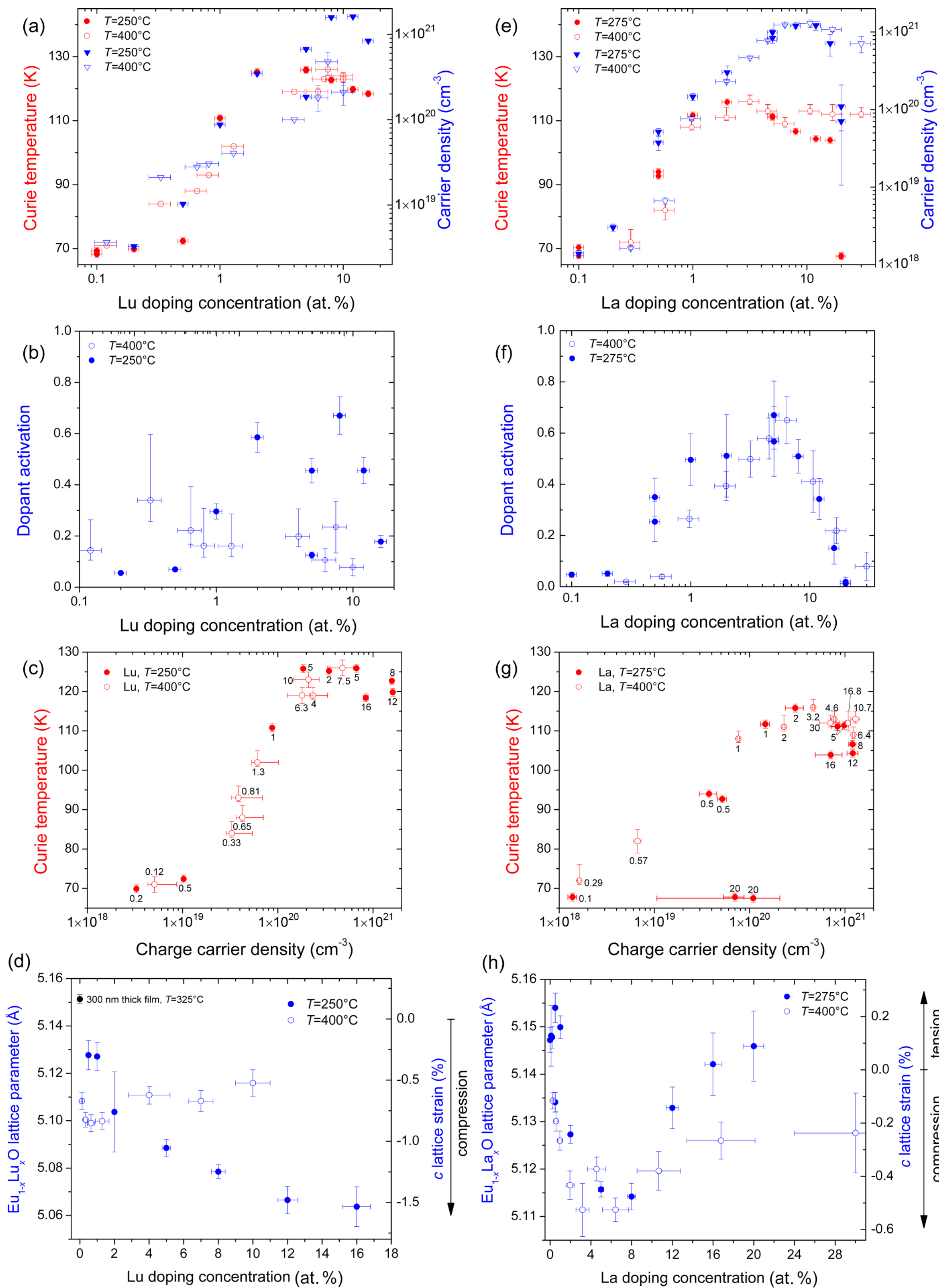

FIG. 1. (a) Dependence of T_C and n on x in $Eu_{1-x}Lu_xO$ films grown at different substrate temperatures T on $LuAlO_3$ and measured at 5 K; (b) calculated dopant activation p as a function of the doping concentration in atomic percent in $Eu_{1-x}Lu_xO$ for the same samples. (c) Dependence of T_C on n in $Eu_{1-x}Lu_xO$ films grown at different substrate temperatures T measured at 5 K. The numbers at the data points denote the doping concentrations in atomic percent. (d) $Eu_{1-x}Lu_xO$ out-of-plane lattice spacing c and calculated c lattice strain as compared to bulk EuO as functions of x, derived from the 002 peak positions in θ-2θ scans. The full symbols represent data points of samples grown at $T = 250\,^{\circ}$C and the empty symbols represent data points of samples grown at $T = 400\,^{\circ}$C. For comparison, the measured c axis of a 300-nm-thick undoped EuO film grown on $LuAlO_3$ at $T = 325\,^{\circ}$C is included. At this thickness, this film is expected to be relaxed [20]. (e)–(h) show the same measurements and calculation results as (a)–(d) but with $Eu_{1-x}La_xO$ films. Please note that the lower growth temperature of these samples was $T = 275\,^{\circ}$C.

grown at $T = 250\,^{\circ}$C reach a maximum activation of up to 67%. In the doping regime where high-T_C values are reached the difference is even more pronounced. Not all of the low-temperature grown samples exhibit high carrier densities and dopant activations, suggesting a strong influence of growth details on these properties. It is worth noting that the low dopant activation of Lu-doped samples grown at $T = 400\,^{\circ}$C is consistent with the low dopant activation previously reported for Gd-doped samples grown in the adsorption-controlled growth regime [22–24].

The data in Fig. 1(c) also show that the T_C of all samples intially strongly increases with increasing n above a threshold of $\sim 5 - 10 \times 10^{18}$ cm^{-3}. Up to $n \sim 2 \times 10^{20}$ cm^{-3} samples with higher n typically also exhibit the higher T_C. This trend continues for the samples grown at $T = 400\,^{\circ}$C up to the highest n values that are reached (4.7×10^{20} cm^{-3}). It becomes clear, however, from the samples grown at lower temperature that reach higher carrier densities, that T_C ultimately levels out at $\sim$126 K, $n = 2 - 5 \times 10^{20}$ cm^{-3}, and 2%–8% doping *concentration* and does not reach higher values, even for much higher n (up to $\sim 1.6 \times 10^{21}$ cm^{-3}). For higher doping concentrations T_C is reduced, despite the very high $n \sim 8 \times 10^{20}$ cm^{-3} of the samples grown at $T = 250\,^{\circ}$C.

Therefore, increasing n beyond $\sim 2 \times 10^{20}$ cm^{-3} does not lead to higher T_C values of these films, as can be inferred from the overall trend and exemplified at the two 5%-doped samples grown at $T = 250\,^{\circ}$C that have strongly differing n (1.9×10^{20} cm^{-3} vs 6.7×10^{20} cm^{-3}), but exactly the same T_C of 126 K.

What other effects could play a role for the observed maximum in T_C? By analyzing the 002 peak positions in θ-2θ scans of the Lu-doped samples grown at $T = 250\,^{\circ}$C on $LuAlO_3$ [Fig. 1(d)] we found an increasing c lattice compression (the out-of-plane direction) of up to -1.6% for the samples grown at $T = 250\,^{\circ}$C as a function of increasing doping concentration. For the EuO bulk lattice parameter we used $a = 5.1439$ Å [29]. The lattice compression of the samples grown by adsorption control shows a different behavior and is almost constant around -0.7%. Interestingly, despite this difference in c-axis strain, the maximum T_C of the samples is the same and the T_C of the samples grown at $T = 250\,^{\circ}$C is already close to the maximum value for 2%–5% doping concentration, although the lattice compression is still increasing for higher x.

To investigate possible effects of dopant ion size we also measured T_C and n of two series of La-doped EuO films deposited on $YAlO_3$, one grown at $T = 400\,^{\circ}$C using standard adsorption-controlled growth and one grown close to the flux-matched regime, at $T = 275\,^{\circ}$C [Fig. 1(e)]. When substituted for Eu^{2+} in the EuO lattice, lanthanum is expected to be in a 3+ valence state just like lutetium, so that it should also donate one electron per ion. With an ionic radius of 1.03 Å it is, however, about 20% larger than the Lu^{3+} ion and closer to the size of Eu^{2+} (1.17 Å) [30].

Remarkably, the La-doped samples reach high charge carrier densities of up to 1.4×10^{21} cm^{-3}, independent of the growth temperature—but the maximum T_C of both sample batches is $\sim$114 K, about 12 K lower than the maximum T_C of the Lu-doped samples. The peak in T_C is reached at 2%–4% doping concentration, far before the peak in n is reached at 10%–12% doping concentration. These effects clearly show that in La-doped as well as Lu-doped EuO high n values are insufficient for reaching high maximum T_C values. At doping concentrations >4%, the T_C of the low-temperature grown La-doped samples is reduced by similar amounts as the low-temperature grown Lu-doped samples, whereas the T_C of the samples grown by adsorption control is reduced by smaller amounts.

The maximum dopant activation of the two La-doped sample batches grown at different temperatures is comparable [Fig. 1(f)]. The dopant activation of the samples grown at lower temperature is only higher for doping concentrations $\sim$0.5% $-$ 2%. Therefore, growth temperature plays a much less important role for the maximum n in La-doped EuO as compared to Lu-doped EuO.

When plotted as a function of n [Fig. 1(g)], the T_C of the La-doped samples initialy shows a strong increase above a threshold of $n \sim 2 - 7 \times 10^{18}$ cm^{-3} and a saturation for $n \gtrsim 3 - 5 \times 10^{20}$ cm^{-3}, similar to the Lu-doped samples. In this n range, samples with higher n also typically exhibit the higher T_C, just like the Lu-doped samples. An exception is very highly La-doped samples (20%) grown at $T = 275\,^{\circ}$C that show enhanced carrier densities, but low T_C values of $\sim$68 K. The RHEED patterns of these samples changed during growth indicating that a structural change of the films due to the high doping is likely responsible for the low T_C. At high n and high x, T_C is reduced—an effect that is more pronounced for the samples grown at lower temperature and is also found in Lu-doped samples [Fig. 1(c)].

The reduction of T_C at doping levels higher than 2%–8% for Lu and 2%–4% for La could be rooted in the weakening of the direct exchange between Eu^{2+} ions caused by the disturbance of the magnetic lattice as expected in case of doping with nonmagnetic ions. The larger lattice compression found for Lu-doped samples as compared with La-doped samples grown at low substrate temperature (see below) may partially alleviate this effect so that T_C is not reduced before reaching higher x values. It should be noted that for Gd doping, T_C has been found to increase up to higher concentrations (at least 10%) [22], as may be expected due to the magnetism of the Gd^{3+} ion. The same effect could be responsible for the slightly higher maximum T_C found for Gd-doped samples (129 K, [22]) as compared to Lu-doped samples (126 K) and the less pronounced drop in T_C for high x in these samples as compared to Lu- and La-doped samples.

Analysis of the c lattice spacing reveals that the lattice compression caused by La doping of EuO films grown at $T = 275\,^{\circ}$C and $T = 400\,^{\circ}$C on $YAlO_3$ reaches a maximum of -0.6% around 6% doping [Fig. 1(h)]. This maximal compressive strain is considerably smaller than the compression of Lu-doped films grown at $T = 250\,^{\circ}$C on $LuAlO_3$ (-1.6% at 16% doping). Due to the 20% larger La ion size this direction of this effect is expected; however, the magnitude is surprisingly large. At high doping concentrations >8% the lattice compression of all the La-doped films is reduced, whereas the lattice of the low-temperature grown Lu-doped samples gets increasingly compressed up to the highest investigated concentration of 16%. It is not yet clear what causes this effect (for possible reasons see the Supplemental Material [27]).

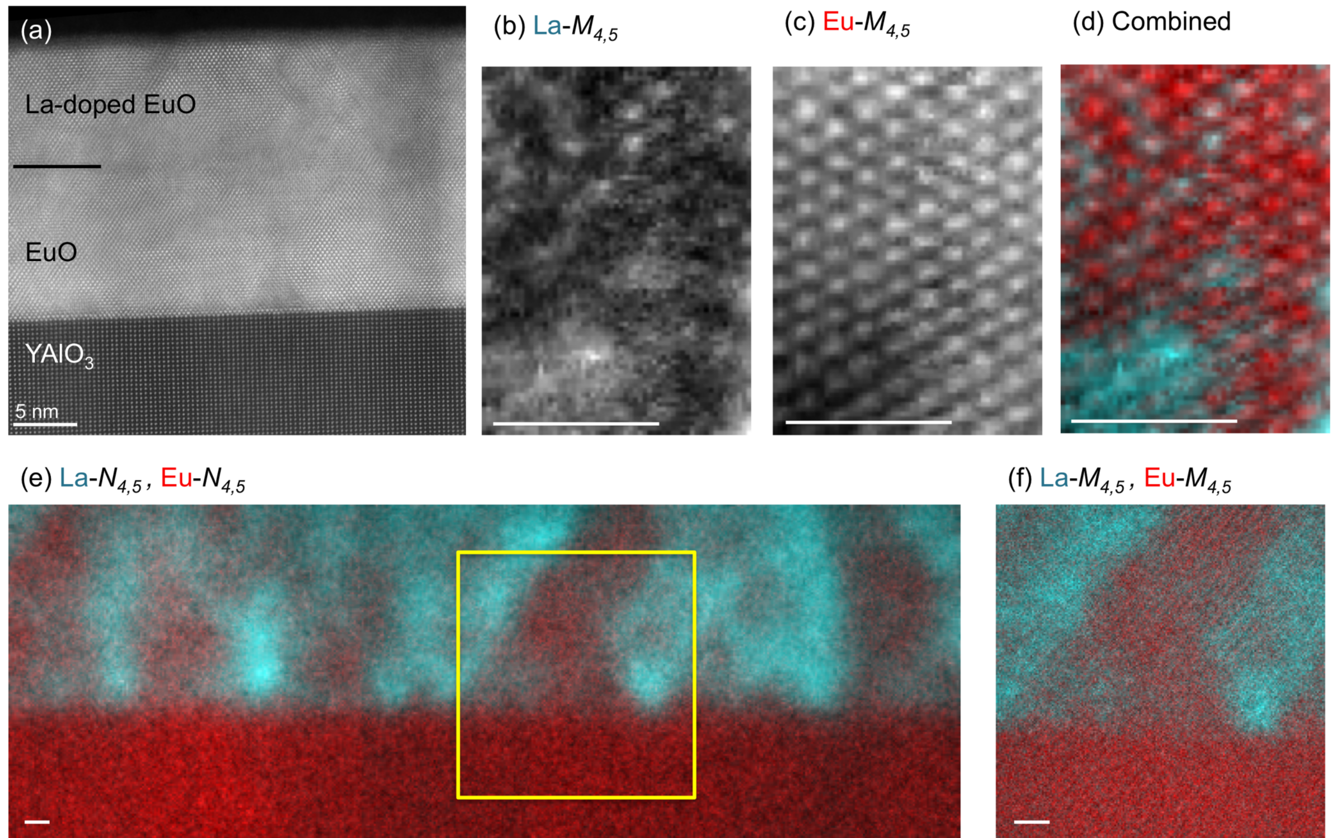

FIG. 2. Spectroscopic imaging of a $La_{0.08}Eu_{0.92}O$ film grown on an undoped EuO buffer layer on a $YAlO_3$ substrate in the adsorption-controlled growth regime. (a) HAADF-STEM image of the sample. Atomic-resolution spectroscopic images of the $La_{0.08}Eu_{0.92}O$ region using the signal from the La-$M_{4,5}$ and Eu-$M_{4,5}$ edges are shown in (b) and (c), respectively. (d) The combined spectroscopic image with lanthanum in turquoise and europium in red shows that the lanthanum signal is inhomogeneous, indicating clustering of lanthanum atoms. (e) A low-magnification EELS spectroscopic image using the La-$N_{4,5}$ and Eu-$N_{4,5}$ edges demonstrates that the lanthanum preferentially clusters the near [010] and [100] zone axes. (f) A high-resolution image of a selected region from (e). Scale bars in (b)–(f) are 1 nm.

Altendorf previously found an approximately linear c-axis lattice contraction with increasing doping concentration in XRD measurements of Sc-doped EuO [17]. The ionic radius of Eu^{2+} is 1.17 Å, as compared to 0.86 Å for Lu^{3+}, 1.03 Å for La^{3+}, and 0.75 Å for Sc [30]. As La^{3+}, Lu^{3+}, and Sc^{3+} are chemically very similar, the smaller Lu^{3+} and Sc^{3+} ion sizes and concomitant stronger lattice compression should also contribute to the higher T_C found in these samples.

Dopant deactivation in conventional semiconductors such as silicon is an issue that has been studied with a large variety of techniques in a vast amount of literature (see, e.g., Ref. [31] and references therein). One of the most important effects leading to the deactivation of dopant carriers is defects in the crystallographic microstructure, the formation of which can depend on film growth conditions, doping level, and the individual dopant/host combination. Therefore, the interdependencies of doping level, density of free carriers, and Curie temperature ideally should also be related to film microstructure when studying dopant deactivation in EuO.

High-angle annular dark field STEM (HAADF STEM) has previously been used to identify individual dopant atoms, e.g., antimony dopant location and clustering in highly doped silicon ($n = 9.35 \times 10^{20}$ cm^{-3}) [32]. In that case, the high atomic number contrast between the antimony ($Z = 51$) and the host silicon ($Z = 14$) led to a large contrast in HAADF STEM; here the dopant atoms (La, $Z = 57$ and Lu, $Z = 71$) have an atomic number similar to europium ($Z = 63$), which makes it harder to locate individual dopant atoms. We thus use two-dimensional (2D) EELS spectroscopic imaging to determine the dopant positions.

Indeed the combination of HAADF STEM and EELS has been successfully used to discern valence changes of the EuO at the EuO/Si interface indicating the formation of impurity phases [33]. Here we use the same techniques to investigate the dopant distribution and dopant cluster formation in La-doped EuO films. We focus on lanthanum doping as the La-$N_{4,5}$ and La-$M_{4,5}$ EELS edges used precede the corresponding Eu-$N_{4,5}$ and Eu-$M_{4,5}$ edges; in contrast, the Lu-$N_{4,5}$ and Lu-$M_{4,5}$ edges sit on the background of the corresponding europium edges making detection of small dopant quantities more difficult. Doping concentrations were between 5% and 8%, as the maximum in T_C for the La-doped samples occurs in this doping range. The La-$M_{4,5}$ and Eu-$M_{4,5}$ edges were used to probe the atomic-scale clustering and the La-$N_{4,5}$ and Eu-$N_{4,5}$ edges to acquire images with a wide field of view at lower spatial resolution.

A HAADF STEM image of an 8% La-doped EuO film grown in the adsorption-controlled regime is shown in Fig. 2(a) (see the Supplemental Material [27] for more

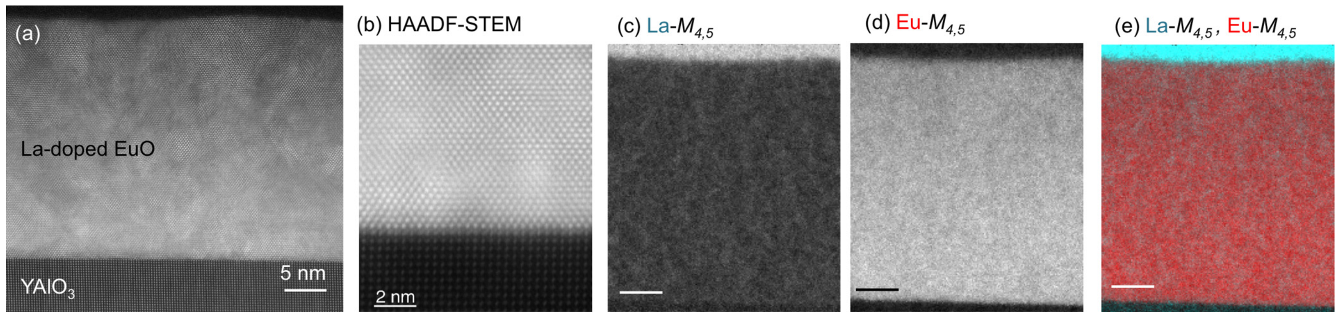

FIG. 3. STEM EELS of an 8% La-doped EuO film grown close to the flux-matching regime at a relatively low substrate temperature of $T = 275\,^{\circ}\mathrm{C}$. (a) Overview image of the sample. The top 12 nm of the EuO film has been oxidized (see Supplemental Material [27]). (b) Atomic-resolution HAADF-STEM image, demonstrating that the interface between the film and the substrate lacks impurity phases. Chemical maps of the lanthanum (c) and europium (d) show homogeneous distribution of these elements. (e) shows a combined color map of the film with lanthanum in turquoise and europium in red. The La content of the $LaAlO_3$ capping layer (bright turquoise) is 20%. Scale bars in (c)–(e) are 5 nm.

information). In Figs. 2(b)–2(d), we show atomic-resolution images of the lanthanum and europium concentrations; even in this small field of view, there is significant fluctuation in the lanthanum concentration ranging from atomic columns with nearly full occupancy of europium to those with nearly 20% lanthanum. This variation was observed over larger fields of view at both atomic and low resolution in Figs. 2(d) and 2(f), respectively. There we note that not only do the lanthanum atoms cluster, they do so along preferred [100] and [010] zone axes. Note that signs of this dopant clustering are not evident in θ-2θ scans or rocking curve XRD measurements.

While the exact nature and electronic structure of the clusters in La-doped EuO remain to be investigated, the extended dopant clustering indicates that such defects could play an important role in dopant deactivation, at least in the doped EuO films grown by adsorption control that tend to exhibit lower dopant activation values. We note that in silicon, pronounced dopant clustering is considered to be one of the main reasons for dopant deactivation at high dopant concentrations $n \sim 1 \times 10^{21}\ \mathrm{cm}^{-3}$ [34].

Dopant clustering could also explain the smaller T_C reduction found in samples grown by adsorption control as compared to low-T grown samples at high La doping levels [Fig. 1(e)]. Even at high doping levels there are regions in the samples grown by adsorption control that contain lower La concentrations (where T_C is maximal), resulting in these high, but inhomogeneously doped samples exhibiting high T_C (Fig. 2). In contrast to these samples, the lower-T grown samples exhibit an almost homogeneous dopant distribution (described below), which obviously leads to a T_C reduction at high La doping levels. Finally, clustering may also influence the lattice parameters of the films and could explain the smaller c-axis lattice compression observed in samples grown by adsorption control.

In Fig. 3 we present an STEM EELS image of an 8% La-doped EuO film grown at $T = 275\,^{\circ}\mathrm{C}$. As shown in Fig. 3(a) and in higher resolution in Fig. 3(b), the film is crystalline and the region between the film and substrate is free of impurities. In contrast to the film grown by adsorption control, the EELS spectroscopic images of the lanthanum and europium edges in Figs. 3(c)–3(e) show a homogeneous lanthanum concentration without significant dopant clustering. The dopant activation in this sample is much higher than the activation typically found in Gd-doped films, but at $p = 58\%$ it is still far from complete.

The finding of extended dopant clustering in La-doped EuO films grown with the growth technique that is most commonly used today—adsorption control—could be part of the explanation of the very low dopant activation values typically found in *some* doped EuO samples. Using lower growth temperatures we were able to avoid the formation of these defects, but the dopant activation still saturated at values below 80%, which is insignificantly higher than the dopant activation values of the *best* La-doped samples grown by adsorption control. Obviously, there must be other mechanisms leading to carrier deactivation that we cannot detect in our STEM-EELS studies.

In this work we have also shown that only low-temperature, close to flux-matched growth allows achieving high lutetium activation. Thermally activated defect formation therefore suggests itself as reason for the difference in carrier deactivation in these Lu-doped films. As lanthanum and lutetium are chemically very similar, but the ionic radius of Lu^{3+} (0.86 Å) is much smaller than that of La^{3+} (1.03 Å) [30], we conclude that small ion size enhances growth-temperature-related deactivation effects in rare-earth doped EuO. This is consistent with the data on Gd-doped EuO published by Mairoser *et al.* [24] who also found a strong reduction of dopant activation with increasing growth temperature. As Gd^{3+} (0.938 Å, [30]) is also smaller than La^{3+}, we postulate that the same effect as in the case of Lu doping is responsible for the low activation of Gd reported by these authors [22,24].

What kinds of defects may lead to these effects? One possibility is vacancies on the Eu site, because rather than two lanthanum dopants giving rise to two mobile electrons ($2\,\mathrm{La}_{\mathrm{Eu}}^{\blacksquare} + 2e'$) the free electrons can instead be fully compensated by the formation of a vacancy on the Eu site ($2\,\mathrm{La}_{\mathrm{Eu}}^{\blacksquare} + V_{\mathrm{Eu}}''$). Such vacancies therefore reduce the number of free electrons. The formation of such defects would be expected to be more pronounced at higher growth temperatures, at which more Eu atoms have enough kinetic energy to leave the growing crystal surface. Smaller dopant ion size would probably strengthen this effect by lowering the formation energy of such defects, because the required EuO lattice

distortions would be smaller. Both of these effects would be consistent with our findings.

Consequently, low deposition temperatures and avoiding O_2 excess is expected to reduce the number of these defects, which should increase the density of free carriers. This effect therefore could explain the very high dopant activation values found in our low-temperature grown samples. It should be observable especially at low doping levels where even a small number of free carrier deactivating defects will lead to a strong reduction or even complete inactivation of free carriers. Indeed, Averyanov *et al.* [35] found recently that using relatively low deposition temperatures ($T \sim 430\,^{\circ}$C) and careful calibration of europium and O_2 fluxes allowed generating significant free carrier densities in Gd-doped EuO films already at very low doping levels <0.05%.

Other effects, which are known from conventional semiconductors, such as donor deactivation distortions of the host lattice, could also play a role here [34]. A theoretical analysis of the energies of formation of different defect states and their effect on dopant deactivation could be highly useful to identify the mechanisms responsible for the dopant deactivation in EuO.

IV. CONCLUSIONS

What conclusions can we draw from these results for the quest of reaching higher Curie temperatures of EuO by rare-earth doping? Our electrical and magnetic measurements reveal that increasing the carrier density in La- and Lu-doped samples does not always result in higher maximum T_C values. We were able to triple the maximum dopant activation in Lu-doped EuO thin films in the regime of high dopant concentrations and Curie temperatures by our low-temperature growth method. This led to unprecedented high carrier densities of up to 1.6×10^{21} cm^{-3}. Unfortunately, increases in n did not result in higher T_C. From the data we conclude that carrier densities in the wide range between 2×10^{20} cm^{-3} and 1.6×10^{21} cm^{-3} neither lead to enhanced nor significantly reduced T_C in these samples. In this range neither n nor T_C depends on n or other effects compensating the effect of n on T_C.

Despite high dopant activation and comparable n, La-doped samples exhibit maximum T_C values of only $\sim$114 K, about 12 K lower than Lu-doped samples grown at 250 °C. La^{3+} and Lu^{3+} ions are both nonmagnetic, so the reason for the T_C difference cannot be due to differences of the disturbance of the magnetic lattice in EuO. Additionally, in combined STEM-EELS measurements we did not find any extended defects that could be responsible for the lower T_C of the low-temperature grown La-doped samples. Further, the sample quality according to XRD is comparable.

Lattice compression is expected to have a considerable influence on T_C [19] and a comparison of x-ray absorption spectroscopy (XAS) measurements with band-structure calculations led to the suggestion that lattice compression underlies the high T_C of Gd-doped EuO [36]. The difference in the c-axis contraction between La- and Lu-doped EuO that we measured by XRD is only -0.2% for the high-T_C samples and too small to account for the full effect. Local strain fields that are not detected in standard XRD analysis, but may well be detected by XAS, are therefore probably more important.

The limited potential of n for increasing T_C of La- and Lu-doped EuO and the indications for a lattice compression related enhancement of T_C strengthen the importance of compressive strain in the quest to further enhance the T_C of EuO thin films. Up to now it is unknown if EuO films can indeed be compressively strained with sufficient thickness so that T_C can be enhanced. One reason for this is a lack of suitable substrates. Fabrication of alternative substrate materials such as $LuVO_4$ (-3.4% strain for an epitaxial and commensurate film) may allow testing this approach. According to our results, the T_C enhancement should be strongest in conjunction with doping with small magnetic ions and possibly oxygen vacancies. The low-temperature, close to flux-matched deposition technique developed in this work is ideally suited to further explore these routes.

ACKNOWLEDGMENTS

The work at Cornell was supported by the National Science Foundation (NSF) [Platform for the Accelerated Realization, Analysis, and Discovery of Interface Materials (PARADIM)] under Cooperative Agreement No. DMR-1539918. This work made use of the Cornell Center for Materials Research Shared Facilities, which are supported through the NSF MRSEC program (Grant No. DMR-1719875). Substrate preparation was performed in part at the Cornell NanoScale Facility, a member of the National Nanotechnology Coordinated Infrastructure (NNCI), which is supported by the NSF (Grant No. ECCS-15420819). The work in Augsburg was supported by the DFG (Grant No. TRR 80).

[1] B. T. Matthias, R. M. Bozorth, and J. H. Van Vleck, Phys. Rev. Lett. **7**, 160 (1961).

[2] M. R. Oliver, J. O. Dimmock, A. L. McWhorter, and T. B. Reed, Phys. Rev. B **5**, 1078 (1972).

[3] Y. Shapira, S. Foner, and T. B. Reed, Phys. Rev. B **8**, 2299 (1973).

[4] K. Y. Ahn and M. W. Shafer, J. App. Phys. **41**, 1260 (1970).

[5] P. G. Steeneken, L. H. Tjeng, I. Elfimov, G. A. Sawatzky, G. Ghiringhelli, N. B. Brookes, and D.-J. Huang, Phys. Rev. Lett. **88**, 047201 (2002).

[6] A. Schmehl, V. Vaithyanathan, A. Herrnberger, S. Thiel, C. Richter, M. Liberati, T. Heeg, M. Röckerath, L. Fitting Kourkoutis, S. Mühlbauer, P. Böni, D. A. Muller, Y. Barash, J. Schubert, Y. Idzerda, J. Mannhart, and D. G. Schlom, Nat. Mater. **6**, 882 (2007).

[7] A. G. Swartz, Appl. Phys. Lett. **97**, 112509 (2010).

[8] D. V. Averyanov, C. G. Karateeva, I. A. Karateev, A. M. Tokmachev, A. L. Vasiliev, S. I. Zolotarev, I. A. Likhachev, and V. G. Storchak, Sci. Rep. **6**, 22841 (2016).

[9] C. Caspers, A. Gloskovskii, M. Gorgoi, C. Besson, M. Luysberg, K. Z. Rushchanskii, M. Ležaić, C. S. Fadley, W. Drube, and M. Müller, Sci. Rep. **6**, 22912 (2016).

[10] D. V. Averyanov, I. S. Sokolov, A. M. Tokmachev, I. A. Karateev, O. A. Kondratev, A. N. Taldenkov, O. E. Parfenov,

and V. G. Storchak, J. Magn. Magn. Mater. **459**, 136 (2018).

[11] T. Mairoser, J. A. Mundy, A. Melville, D. Hodash, P. Cueva, R. Held, A. Glavic, J. U. R. Schubert, D. A. Muller, A. Schmehl, and D. G. Schlom, Nat. Commun. **6**, 1 (2015).

[12] T. R. McGuire and M. W. Shafer, J. Appl. Phys. **35**, 984 (1964).

[13] F. Holtzberg, T. R. McGuire, S. Methfessel, and J. C. Suits, Phys. Rev. Lett. **13**, 18 (1964).

[14] A. Mauger, M. Escorne, C. Godart, J. P. Desfours, and J. C. Achard, J. Phys., Colloq. **41**, C5 (1980).

[15] K. Y. Ahn and T. R. McGuire, J. Appl. Phys. **39**, 5061 (1968).

[16] A. Melville, T. Mairoser, A. Schmehl, D. E. Shai, E. J. Monkman, J. W. Harter, T. Heeg, B. Holländer, J. Schubert, K. M. Shen, J. Mannhart, and D. G. Schlom, Appl. Phys. Lett. **100**, 222101 (2012).

[17] S. G. Altendorf, Appl. Phys. Lett. **104**, 052403 (2014).

[18] A. Mauger and C. Godart, Phys. Rep. **141**, 51 (1986).

[19] N. J. C. Ingle and I. S. Elfimov, Phys. Rev. B **77**, 121202 (2008).

[20] A. Melville, T. Mairoser, A. Schmehl, T. Birol, T. Heeg, B. Holländer, J. Schubert, C. J. Fennie, and D. G. Schlom, Appl. Phys. Lett. **102**, 062404 (2013).

[21] A. Mauger, Phys. Status Solidi B **84**, 761 (1977).

[22] T. Mairoser, A. Schmehl, A. Melville, T. Heeg, L. Canella, P. Böni, W. Zander, J. Schubert, D. E. Shai, E. J. Monkman, K. M. Shen, D. G. Schlom, and J. Mannhart, Phys. Rev. Lett. **105**, 257206 (2010).

[23] J. M. Riley, F. Caruso, C. Verdi, L. B. Duffy, M. D. Watson, L. Bawden, K. Volckaert, G. van der Laan, T. Hesjedal, M. Hoesch, F. Giustino, and P. D. C. King, Nat. Commun. **9**, 2305 (2018).

[24] T. Mairoser, A. Schmehl, A. Melville, T. Heeg, W. Zander, J. Schubert, D. E. Shai, E. J. Monkman, K. M. Shen, T. Z. Regier, D. G. Schlom, and J. Mannhart, Appl. Phys. Lett. **98**, 102110 (2011).

[25] R. W. Ulbricht, A. Schmehl, T. Heeg, J. Schubert, and D. G. Schlom, Appl. Phys. Lett. **93**, 102105 (2008).

[26] R. Sutarto, S. G. Altendorf, B. Coloru, M. Moretti Sala, T. Haupricht, C. F. Chang, Z. Hu, C. Schüßler-Langeheine, N. Hollmann, H. Kierspel, J. A. Mydosh, H. H. Hsieh, H.-J. Lin, C. T. Chen, and L. H. Tjeng, Phys. Rev. B **80**, 085308 (2009).

[27] See Supplemental Material at http://link.aps.org/supplemental/10.1103/PhysRevMaterials.4.104412 for additional information on the deposition method of EuO thin films at low temperature, measurement of dopant incorporation, structural quality as measured by x-ray diffraction, determination of magnetic and electrical properties, comparison to previous work, and determination of the lanthanum valence in La-doped EuO thin films by STEM EELS.

[28] T. Mairoser, F. Loder, A. Melville, D. G. Schlom, and A. Schmehl, Phys. Rev. B **87**, 014416 (2013).

[29] *Landolt-Bornstein: Numerical Data and Functional Relationships in Science and Technology*, edited by K.-H. Hellwege, New Series, Group III (Springer, Berlin, 1975), Vol. 7, Part b1, p. 33.

[30] R. D. Shannon, Acta Crystallogr., Sect. A **32**, 751 (1976).

[31] P. M. Fahey, P. B. Griffin, and J. D. Plummer, Rev. Mod. Phys. **61**, 289 (1989).

[32] P. M. Voyles, D. A. Muller, J. L. Grazul, P. H. Citrin, and H.-J. L. Gossmann, Nature **416**, 826 (2002).

[33] J. A. Mundy, D. Hodash, A. Melville, R. Held, T. Mairoser, D. A. Muller, L. Fitting Kourkoutis, A. Schmehl, and D. G. Schlom, Appl. Phys. Lett. **104**, 091601 (2014).

[34] D. C. Mueller and W. Fichtner, Phys. Rev. B **70**, 245207 (2004).

[35] D. V. Averyanov, O. E. Parfenov, A. M. Tokmachev, I. A. Karateev, O. A. Kondratev, A. N. Taldenkov, M. S. Platunov, F. Wilhelm, A. Rogalev, and V. G. Storchak, Nanotechnology **29**, 195706 (2018).

[36] S. G. Altendorf, N. Hollmann, R. Sutarto, C. Caspers, R. C. Wicks, Y.-Y. Chin, Z. Hu, H. Kierspel, I. S. Elfimov, H. H. Hsieh, H.-J. Lin, C. T. Chen, and L. H. Tjeng, Phys. Rev. B **85**, 081201(R) (2012).

Supplemental Material

Deposition of Doped EuO Films at Low Temperature

As the oxygen stoichiometry of EuO films cannot directly be measured *in situ* with our setup, we assessed whether RHEED could provide relevant *in situ* feedback on the growth of EuO films at low temperature in a regime where precise flux matching between europium and oxygen molecular beams is crucial. In preliminary experiments ~35 nm thick EuO films were grown at different oxygen partial pressures, $P(O_2)$, and substrate temperatures, T. We found that 35 nm thick films showing no secondary phases in RHEED could be grown at $T = 250 - 275$°C and an Eu flux of 5.79×10^{13} atoms/(cm^{2}s) if the oxygen partial pressure $P(O_2)$ was adjusted to a certain value around 2.5×10^{-8} Torr with an accuracy better than $\pm 2\%$ (Figs S1 and S2). The exact required $P(O_2)$ also depended on the doping concentration and the H, H_2, O, O_2, and H_2O background levels of the chamber.

To test this calibration, three films of undoped EuO were deposited at conditions that lead to either no extra spots or only faint spots in RHEED due to a slight excess of O_2 after the growth of 35 nm thick films. The properties of these films were investigated by magnetometry and transport measurements. The T_C of these samples was measured to be 69.0 K, 69.3 K, and 70.0 K, which is consistent with stoichiometric EuO within the error bar of 1 K. In addition, all three films exhibited electrical resistances >5 GΩ at 5 K. Therefore we conclude that the concentration of oxygen vacancies in EuO can be well controlled by our low-temperature growth technique and is negligible at the deposition conditions used. The same low-temperature deposition technique with *in situ* RHEED control was used to grow all of the doped samples. Films exhibiting spots in RHEED due to the growth conditions being metal-rich were discarded and not used for this study.

The temperature of the europium source was set to provide a Eu flux at the substrate of $(5.5 \pm 0.3) \times 10^{13}$ atoms/cm^{2}s as measured by a quartz crystal microbalance (QCM). Unless $P(O_2)$ was inside of a narrow growth window, extra spots appeared in RHEED after the deposition of a few nanometers of material, indicating the formation of additional phases (Fig. S2). At oxygen partial pressures just a few percent outside of this growth window, the extra spots that appeared could be clearly related to oxygen-rich or oxygen-poor conditions. Changing the growth conditions accordingly in subsequent growth removed the extra spots. For larger deviations from the ideal $P(O_2)$, the extra spots became more clear and with greater deviation were replaced by rings, indicating polycrystallinity.

XRD was less sensitive to oxygen non-stoichiometry than was RHEED. Only if more than 2% overoxidizing growth conditions were maintained over a long time (growth of ~20 nm) was Eu_3O_4 detected in θ-2θ scans. This demonstrated the superior sensitivity of RHEED over XRD for avoiding this unwanted phase. These test samples were capped with 100 nm of polycrystalline aluminum immediately after growth (prior to removing the sample from the MBE and exposing it to air so that XRD spectra could be measured) to avoid overoxidation of the EuO surface after deposition. In other samples sometimes overoxidation was an issue (as described in the section "Structural Quality of the Films as Measured by XRD"). For slightly oxygen-deficient growth conditions that were sufficient to yield characteristic extra spots in RHEED, no additional peaks were observed in θ-2θ scans, even for prolonged growth under these conditions. This indicates the low sensitivity of

standard XRD measurements for clusters of metallic europium. Only samples yielding no extra spots or faint extra spots indicating a small oxygen excess by RHEED were used for this study to minimize the influence of oxygen vacancies on the properties of the measured films.

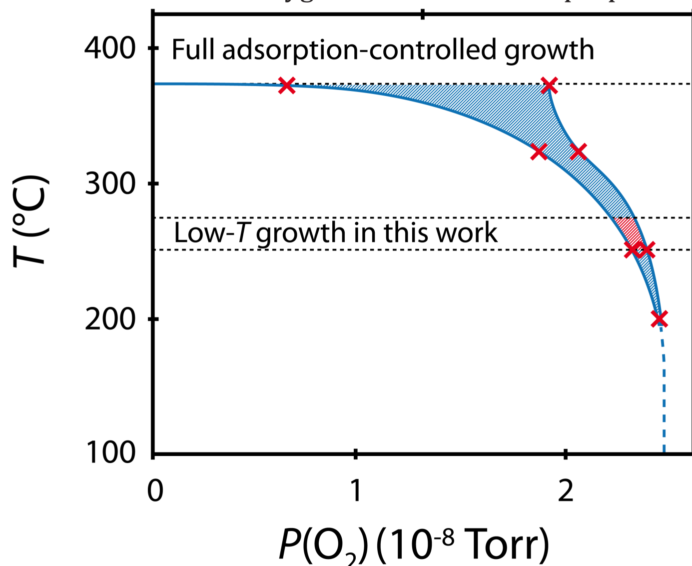

FIG. S1. (Color online) Growth window of close-to-stoichiometric EuO deposited on (110) $YAlO_3$ as determined from RHEED studies as a function of measured substrate heater temperature, T, and estimated absolute oxygen partial pressure, $P(O_2)$, at a constant europium flux of 5.22×10^{13} atoms/(cm^{2}s). The red crosses indicate the $P(O_2)$-limits for the growth of extra-spot-free ~35 nm-thick EuO-films at a given T as determined by RHEED. The blue lines connecting these crosses are guides to the eye. Close-to-stoichiometric EuO could be grown at lower temperatures than needed for adsorption-control (375 °C) within the region shaded in blue; the parameter space used for the low-temperature growth of the main samples of this study is shaded in red.

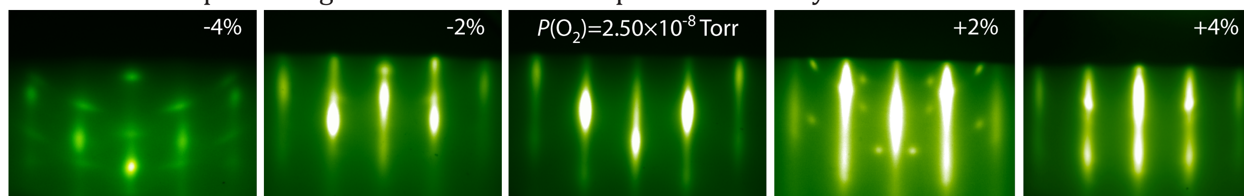

FIG. S2. (Color online) RHEED images with the incident beam along the [110] EuO (or [001] $YAlO_3$) azimuth for ~35 nm-thick EuO films grown on (110) $YAlO_3$ at different oxygen pressures, $P(O_2)$, and substrate temperatures around 250 °C. The percentage values given indicate the deviation of the absolute $P(O_2)$ from extra-spot-free growth at $P(O_2) = 2.50 \times 10^{-8}$ Torr, estimated from ion gauge measurements.

We controlled the oxygen partial pressure $P(O_2)$ using a mass spectrometer (Stanford Research Systems SRS 200). The mass spectrometer allowed relative control of $P(O_2)$ to better than ±1% at the pressures used. As the spectrometer was not calibrated to absolute pressure, we determined these values using a Granville Phillips Stabil-Ion ion gauge and subtracting the background pressure of $\sim 5 \times 10^{-9}$ Torr that was mainly given by the outgassing of H_2 from the hot europium source.

At lower substrate temperatures more and more of the impinging europium atoms stick to the crystal surface, leading to a pronounced narrowing of the growth window between the adsorption-controlled regime (375-400 °C) and ∼200 °C. Below 200°C we were not able to grow ∼35 nm-thick extra-spot-free EuO films on $YAlO_3$ or $LuAlO_3$, as the films quickly became polycrystalline. This may be the result of the narrowing of the growth window or to the limited thermal energy available for surface diffusion of the adatoms during crystallization of EuO on these substrates.

The highly insulating behavior of undoped EuO grown with this method at low temperatures (R>5 GΩ at 5 K) and the unaltered T_C of 69 ± 1 K of these samples indicates that this growth method can be used to grow EuO films with a stoichiometry that is very close to ideal. Additionally, this method also provides a way to intentionally grow oxygen-deficient or overoxidized samples with well-controlled deviations from the EuO stoichiometry by varying the O_2 partial pressure or the europium flux. It could therefore be used to investigate the influence of oxygen vacancies on the properties of undoped and doped EuO films.

The method that we have used can be viewed as an extension of the method recently reported for the growth of undoped and Gd-doped EuO films at a temperature very close to the edge of full adsorption control (T∼430 °C) [1]. Undoped films grown in this regime by Averyanov *et al.* [1] using careful calibration of europium and O_2 fluxes showed unprecedentedly large metal–insulator transitions with a change in resistivity of 11 orders of magnitude. Gd-doped samples grown under these conditions showed a transition from semiconducting to metallic transport characteristics already at very low doping levels of <0.05% [1].

Measurement of Dopant Incorporation for Samples Grown at Different Temperatures

For samples grown with low-temperature, flux-matched conditions it can be assumed that the intended doping ratio is transferred to the sample, because almost all impinging atoms stick to the growing film surface, including europium and the dopant element. In the adsorption-controlled growth regime, however, the EuO growth rate is variable and determined by the actual oxygen partial pressure, whereas the lutetium and lanthanum dopant atoms typically stick to the growing film surface. This was found in RHEED studies that were performed up to $T = 550$ °C, a much higher temperature than the temperatures used for thin film deposition in this study. This effect can lead to undesired deviations from the intended doping level for films deposited in the adsorption-controlled regime if $P(O_2)$ is not controlled with sufficient precision. Therefore, we measured the areal densities of europium atoms in samples grown by adsorption control by Rutherford backscattering spectrometry (RBS), compared them to the expected values, and corrected the actual dopant concentration accordingly. For the 7% and 10% Lu-doped samples we were able to directly determine the doping concentration from the RBS spectra.

Substrates

We used two materials with the perovskite structure as substrates, (110) $YAlO_3$ and (110) $LuAlO_3$. They are both excellent insulators that preclude shunting in the Hall measurements. The band gap of $YAlO_3$ is ∼7.5 eV [2]; the band gap of $LuAlO_3$ is ∼8.4 eV at 10 K [3]. Both materials are orthorhombic. The rectangular surface net of (110) $LuAlO_3$ has an in-plane lattice constant of 7.379 Å along the $[1\bar{1}0]$ direction and 7.300 Å along the [001] direction. For (110) $YAlO_3$, these in-plane

distances are 7.432 Å and 7.370 Å, respectively. The expected epitaxial orientation relationship for $LuAlO_3$ is (001) EuO ∥ (110) $LuAlO_3$ with $[1\bar{1}0]$ EuO ∥ [001] $LuAlO_3$ and [110] EuO ∥ $[1\bar{1}0]$ $LuAlO_3$, with a linear lattice mismatch of +0.4% and +1.5% along the EuO $[1\bar{1}0]$ and [110] directions, respectively [4]. The epitaxial relationship for EuO growth on $YAlO_3$ is equivalent, with slightly larger linear lattice mismatches of +1.3% and +2.2%, respectively [5].

XRD analysis of highly La-doped films ≥8% shows comparable FWHM of rocking-curves as for Lu-doped films and no indications of other phases in θ-2θ-scans. It could be that the larger tensile in-plane strain imposed by the $YAlO_3$ substrates (+1.8%) as compared to the $LuAlO_3$ substrates (+1.0%) leads to the relaxation of the compressive *c*-axis strain of the La-doped EuO films at relatively low doping levels. The early relaxation of La-doped EuO could also be related to the formation of characteristic microstructural defects. Further studies are needed to clarify this point.

Structural Quality of the Films as Measured by XRD

The crystalline quality of the films was investigated by XRD using θ-2θ scans and rocking curve scans in ω. The θ-2θ scans of some samples showed small additional peaks at locations consistent with Eu_3O_4 or Eu_2O_3 (Figs. S3-S6). No peaks were seen at positions consistent with lutetium or lanthanum metal or Lu_2O_3, La_2O_3, silicon (capping), or $LaAlO_3$ (capping). As samples grown using both low-temperature and adsorption-controlled conditions showed the additional peaks seen in Figs. S3-S6, we attribute the formation of these peaks to phases involving excess oxidation either from the oxygen background to which the samples were exposed prior and during capping with amorphous $LaAlO_3$ or during sample transfer into the vacuum chamber in which the capping with amorphous silicon occurred.

This is corroborated by the STEM-EELS measurements of the 8% La-doped sample grown at low temperature that was capped with amorphous $LaAlO_3$. It shows a higher than Eu^{2+} oxidation state only at the EuO-capping layer interface and no other detectable phases (Fig. 6). In a θ-2θ scan of this sample we found a small peak indicating the presence of Eu_3O_4 in the film. Consistent with this finding, STEM-EELS shows that about 12 nm of the EuO at the interface to the $LaAlO_3$ capping layer reacted to raise the oxidation state of the Eu^{2+}, probably during the deposition of the capping layer, which involves oxygen pressures about 100 times higher than that used for the growth of the EuO film.

The bulk of the film is free of phases that are more oxidized than EuO, as indicated by the homogeneity of the measured Eu^{2+} valence. Differences in the intensities of the observed impurity peaks in XRD are likely caused by small alignment differences of the films, differing oxygen backgrounds before capping, and differences in roughness of the films that can lead to varying surface areas and oxidation rates. The roughness of the samples grown at low temperature increased considerably as observed by RHEED, especially for those with lutetium doping levels ≥8%,. Also the roughness of the Lu-doped samples grown under adsorption-controlled conditions increased at high doping levels as indicated by the missing thickness fringes around the EuO 002 peak in the θ-2θ scans. Taking the partial surface degradation of the Lu-doped samples that were grown at low temperature into account, the carrier densities of some of the samples probably were slightly higher than actually measured, due to overestimation of the active film thickness.

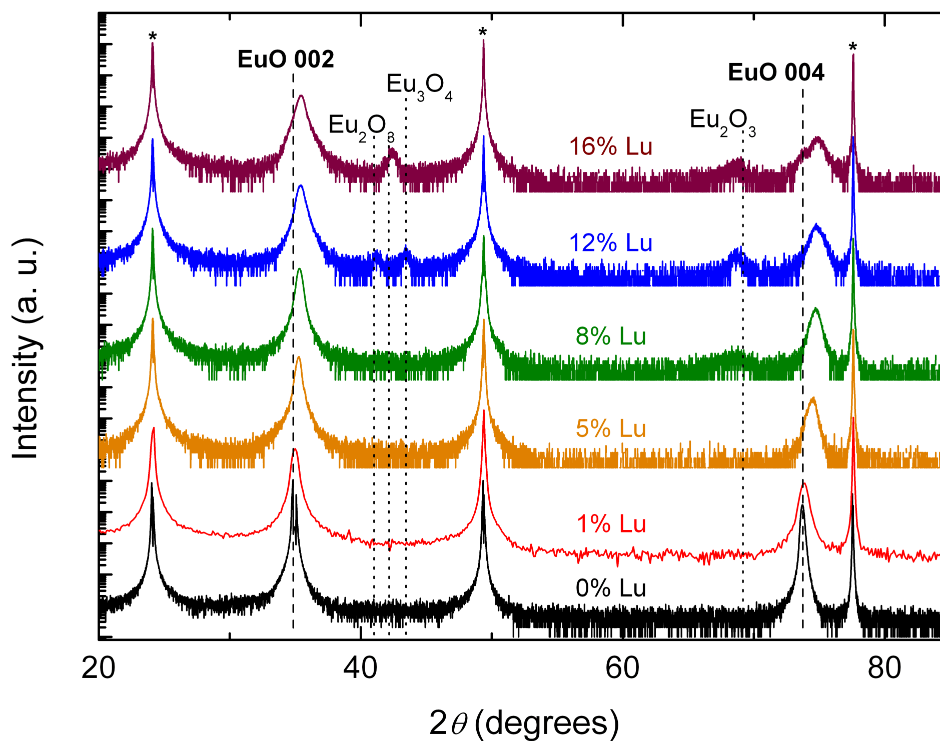

FIG. S3 (color online) θ-2θ scans of $Eu_{1-x}Lu_xO$ films deposited on $LuAlO_3$ substrates at low temperature and capped with ~100 nm of amorphous silicon. The scans are offset along the intensity axis for clarity. Substrate peaks are indicated with asterisks. The positions of various Eu_3O_4 and Eu_2O_3 peaks are also marked. Samples used for calibration of $P(O_2)$ were capped *in situ* with aluminum, which required no oxygen background during capping and no sample transfer. Samples that did not show any extra spots in RHEED and were capped *in situ* with aluminum did not show any additional peaks in XRD.

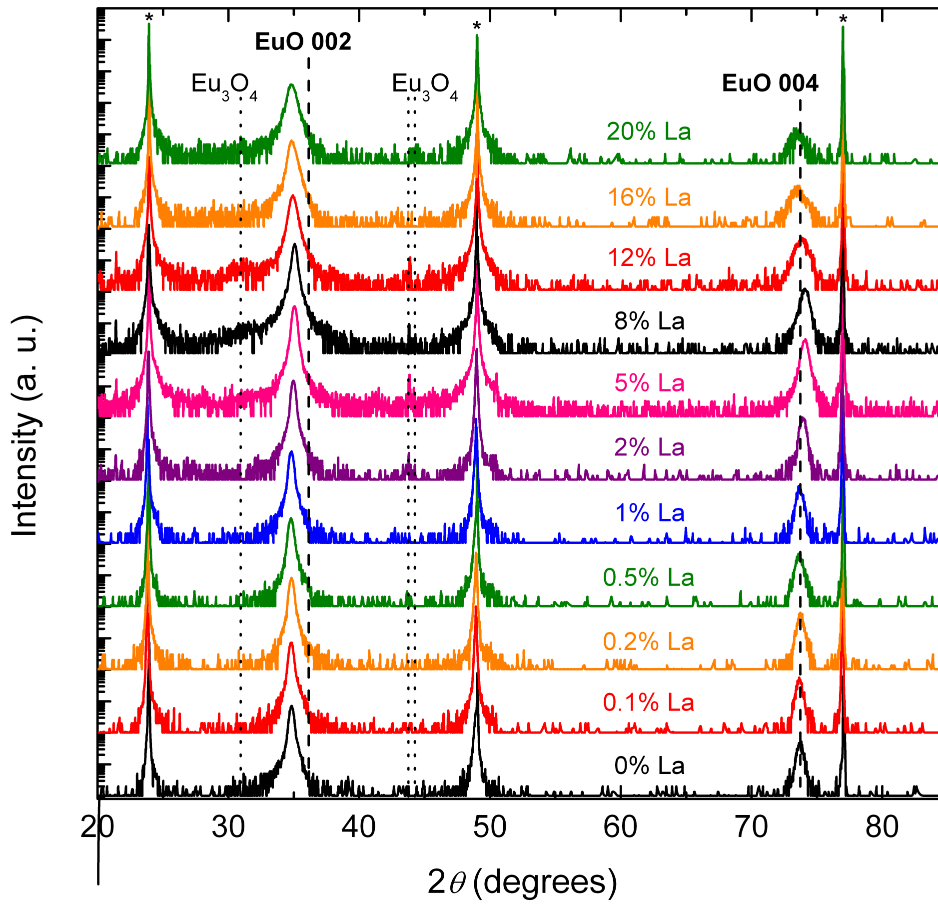

FIG. S4. (Color online) θ-2θ scans of $Eu_{1-x}La_xO$ films deposited on $YAlO_3$ substrates at low temperature and capped with ~100 nm of amorphous $LaAlO_3$. The scans are offset along the intensity axis for clarity. Substrate peaks are indicated with asterisks. The positions of the relevant Eu_3O_4 peaks are also marked.

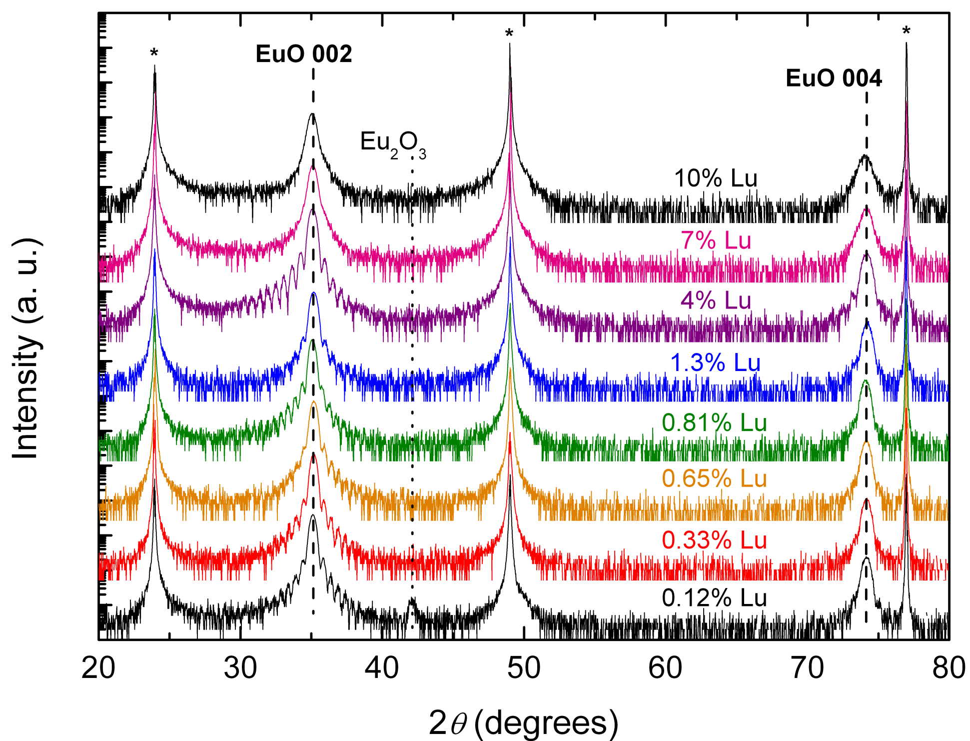

FIG. S5. (Color online) θ-2θ scans of $Eu_{1-x}Lu_xO$ films deposited on $YAlO_3$ substrates at 400 °C (adsorption-controlled conditions) and capped with ~100 nm of amorphous silicon. The scans are offset along the intensity axis for clarity. Substrate peaks are indicated with asterisks. The position of a relevant Eu_2O_3 peak is also marked.

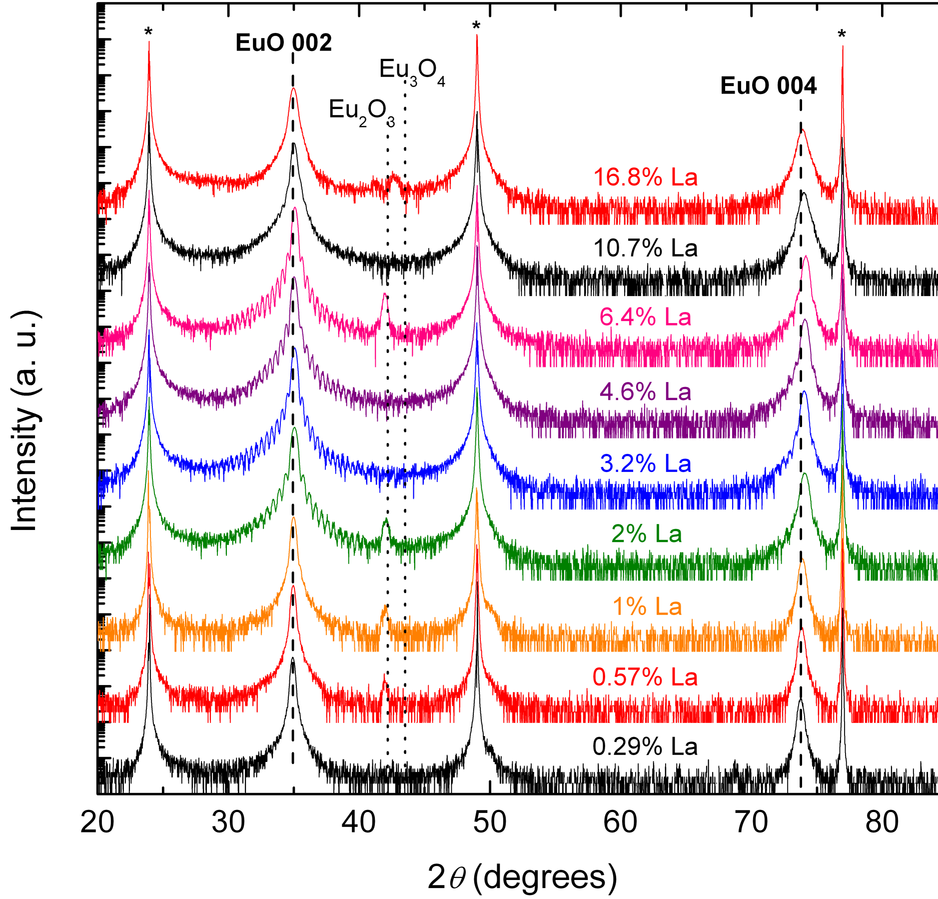

FIG. S6. (Color online) θ-2θ scans of $Eu_{1-x}La_xO$ films deposited on $YAlO_3$ substrates at 400 °C (adsorption-controlled conditions) and capped with ~100 nm of amorphous silicon. The scans are offset along the intensity axis for clarity. Substrate peaks are indicated with asterisks. The positions of various Eu_3O_4 and Eu_2O_3 peaks are also marked.

With FMHW values between 0.12° and 0.73°, the rocking curves of the Lu-doped samples grown at low temperature are about ten times broader than the rocking curves of the adsorption-controlled samples (FWHM ≤0.07°, see Fig. S7). We find about the same difference in FWHM for the rocking curves of the La-doped samples grown in these two different regimes (FWHM 0.12-0.95° vs. FWHM ≤0.04°). Possible reasons for the inferior crystallinity of the samples grown at lower temperature are the smaller thermal energy available for crystallization and possible slight oxygen-rich growth conditions that were chosen to avoid oxygen vacancies in the films. It is interesting that, despite the worse crystallinity, the doped films deposited at lower temperature still reach the same or higher maximum T_C values and much higher maximum carrier densities than the films

deposited with adsorption control. Therefore, good crystallinity is clearly not a sufficient criterion for reaching high n, high p, and high T_C.

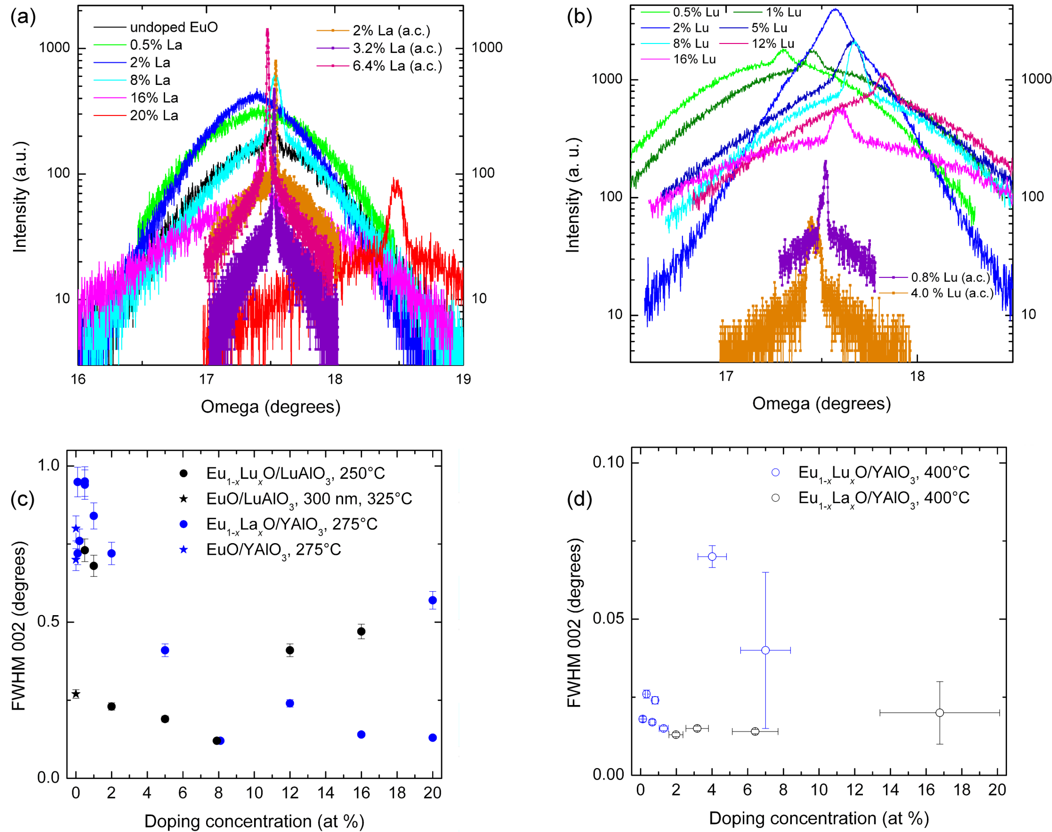

FIG. S7. (Color online) Rocking curves of the 002 peak of (a) $Eu_{1-x}La_xO$ films deposited on $YAlO_3$ substrates, including an undoped EuO film and (b) $Eu_{1-x}Lu_xO$ films deposited on $LuAlO_3$ substrates. a.c. denotes adsorption-controlled growth conditions. The corresponding FWHM of the rocking curves as a function of doping concentration for the films deposited at (c) low temperature and (d) 400 °C (adsorption-controlled conditions). The two data points in (c) at 8% doping concentration are slightly offset along the horizontal axis for clarity.

Magnetic and Electrical Properties and Comparison to Previous Work

We determined the ferromagnetic ordering temperatures T_{FM} of the samples from the $M(T)$ characteristics measured by superconducting quantum interference device (SQUID) magnetometry or vibrating sample magnetometry (VSM). For this purpose, we calculated the negative temperature derivative of the raw data and estimated the position of the high-temperature shoulder of magnetization. Here it should be noted that the T_{FM} and the Curie Temperature T_C values for doped EuO reported by different groups vary widely. As clarified by Mairoser *et al.*, [6] possible reasons for discrepancies include differing measurement methods (e.g., SQUID-magnetometry-based methods, X-ray magnetic dichroism (XMCD), second harmonic generation (SHG), etc.) and the application of varying magnetic background fields during the particular measurements employed. Depending on the dopant element, applied external magnetic fields can indeed lead to an increase of the measured ferromagnetic ordering temperature, T_{FM}, by sizable amounts. Therefore we only used very small external magnetic fields $\mu_0 H < 25$ Gauss for our

measurements. As we expect a negligible influence of this background field on the measured T_{FM}, we assume $T_{FM} = T_C$. Strict slope criteria, that are sometimes used in this context are not supported by underlying physics and falsely suggest certainty. Therefore, we followed the most common way to extract T_{FM} and estimated T_{FM} by eye [6].

The magnetic and electrical properties of La- and Lu-doped samples grown using adsorption-controlled conditions have been reported previously. For example, 5% La- and Lu-doped EuO films deposited under adsorption-controlled conditions showed T_C values of 116 K and 119 K, respectively [7]. Further, 8% La- and Lu-doped samples exhibited T_C values of 116 K and 126 K, respectively [6]. These values are comparable with the values of our corresponding adsorption-controlled samples. The T_C values of nominally 0.5% and 1% La-doped samples reported in [5] of 105 K and 118 K, respectively, are relatively high for the doping level stated. Our samples also reach 118 K within the error bar, but only at 2% doping. This difference may be explained by the relatively high deviation of the estimated doping concentration that is typical when using adsorption-controlled conditions.

The charge carrier densities of the Lu- and La-doped samples grown under adsorption-controlled conditions that we measured by Hall-effect are as high or higher than the values published in previous works ($n_{Lu} = 1.8 \times 10^{20}$ and $n_{La} = 2.1 \times 10^{20}$ at 5% doping [7], $n_{Lu} = 2.1 \times 10^{20}$ and $n_{La} = 1.1 \times 10^{21}$ at 8% doping [6]). In looking at the data of the La-doped samples alone, it seems possible that $n > 2 \times 10^{20}$ cm^{-3}contributes to the reduction in T_C. But taking into account the data on Lu-doped EuO this contribution is probably very small, as n is unimportant for T_C in a wide range of carrier densities in these samples. Theory would also expect only a minor reduction of T_C for $n \gg 3 \times 10^{20}$ cm^{-3} [8].

To measure the Hall resistance R_H at T=5 K at the ~100 μm wide Hall bars we made low resistance contacts by filling ion-etched holes with magnesium and titanium. The mobile charge carrier density, n, was determined from fitting the $R_H(H)$ characteristics for fields well above the saturation field ($4\text{ T} \leq |\mu_0 H_{sat}| \leq 8\text{ T}$), following Ref. [9]. At 5 K, contributions of the anomalous Hall effect to R_H are negligible and the measured n is a very good measure of the free carrier density originating from the dopants [9].

The $M(T)$ curves of our samples grown at low temperatures are presented in Figs. S8-S10. There are anomalies in the 0.2%, 0.5%, and possibly 1% $M(T)$ characteristics of Lu-doped EuO that are probably mostly artifacts from the VSM measurements (Fig. S8). The background field of 2.5 mT used in these measurements is small and the magnetic domain size in EuO is <1 μm [10]. Therefore the $M(T)$ characteristics do not represent the single-domain magnetization of the films. Consequently, small changes in sample position or applied field can lead to temperature-dependent changes in the domain configurations that result in anomalies in the $M(T)$ curves. Despite this effect, the onset of magnetization that was used to determine T_C is clearly visible for all samples. Application of a background field of 1 T removed the anomalies except for a slight double-dome shape of the curves that may indicate the presence of slight phase separation in the films (Fig. S9; please also see the discussion in the next section).

Apart from the artifacts in the low-field measurements, the $M(T)$ curves of Lu-doped samples grown at low temperatures are similar to curves found in the literature [6]. The $M(T)$ curves of the La-doped samples grown at $T = 275$ °C measured by SQUID in zero field do not show any anomalies (Fig. S10). We conclude that the shape of the $M(T)$ curves of low-temperature-grown La- and Lu-

doped EuO is comparable to the shape of La- and Lu-doped EuO grown under adsorption-controlled conditions [6], Gd-doped EuO [9, 11,-13], and Sc-doped EuO [14].

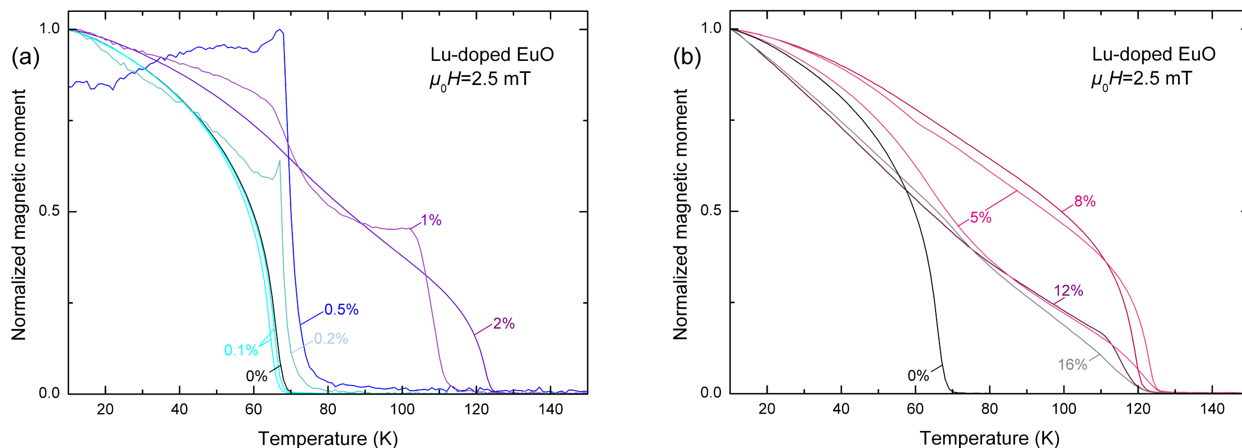

FIG. S8. (Color online) Normalized magnetic moment of $Eu_{1-x}Lu_xO$ films deposited at 250 °C on $LuAlO_3$ substrates as a function of temperature measured by VSM magnetometry at a background field of 2.5 mT; (a) graphs for lutetium doping levels between 0 and 2%; (b) graphs for lutetium doping levels between 0 and 16%.

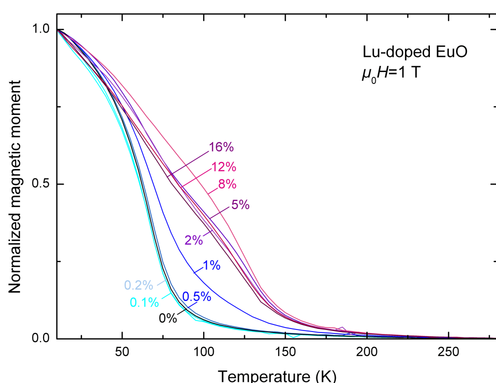

FIG. S9. (Color online) Magnetic moment of $Eu_{1-x}Lu_xO$ films deposited at 250 °C on $LuAlO_3$ substrates as a function of temperature measured by VSM magnetometry at a background field of 1 T.

In previous work, the influence of oxygen deficiency on the shape of the $M(T)$ characteristics of undoped EuO has been investigated [15]. In that work, the films were grown at $T = 200$ °C and $P(O_2)$ was lowered until the samples showed strong extra spots in RHEED, clearly indicating oxygen-poor conditions. At a background field of 0.1 T, a pronounced "tail" was observed in the $M(T)$ curves of those samples that was attributed to the presence of europium metal clusters in the films that align when high magnetic fields are applied. The $M(T)$ characteristics of our Lu-doped films grown at $T = 250$ °C do not show such tails even at a background fields of 1 T (see Fig. S9), indicating the good oxygen stoichiometry of our films and further corroborating the validity of our low-temperature growth method.

In some prior work, a tail has also been observed in $M(T)$ measurements of doped EuO thin films measured in *low* background fields. In the case of Sc-doped films, this effect has been attributed to dopant clustering [14]. We also observe such tails in our samples grown at low temperature, but only at the highest investigated doping level (20% La, Fig. S10b).

Another recurring feature of interest in the $M(T)$ curves of doped EuO is the so-called "double-dome" shape that has, e.g., been attributed to phase separation at scandium doping levels higher and lower than 7% concentration [14]. We also find such features in some of the Lu- and La-doped samples grown at low temperature (Figs. S8 and S10), such as the 8% La-doped EuO film that we also investigated by STEM and EELS. In the STEM-EELS measurements of this sample we did not find any indications of extended clustering, but Hall-effect measurements revealed a far from complete dopant activation of 58%. The samples with the highest dopant activations of around 2/3 (8% Lu and 5% La) show relatively small deviations from the ideal $M(T)$ Brillouin function of undoped EuO. More measurements are necessary to clarify this point, but as there seems to be a tendency towards bigger deviances of the $M(T)$ curve shape from ideal Brillouin functions for samples with lower dopant activations, the appearance of the double-dome feature may indicate the presence of a large number of dopant-deactivating defects in the films. The same mechanism may be responsible for the double-dome shape of some of the $M(T)$ curves of the Lu-doped samples grown at $T = 250$ °C. For example, the $M(T)$ curve of the 5% Lu-doped sample with the higher carrier density and dopant activation ($n = 6.7 \times 10^{20}/cm^3$ and p=46%) more closely resembles a Brillouin function than does the double-dome shaped $M(T)$ characteristic of the 5% Lu-doped sample with n= $1.9 \times 10^{20}/cm^3$ and p=13% that was grown under slightly oxygen-rich conditions as indicated by RHEED. These 5% Lu-doped samples are both shown in Fig. S8(b).

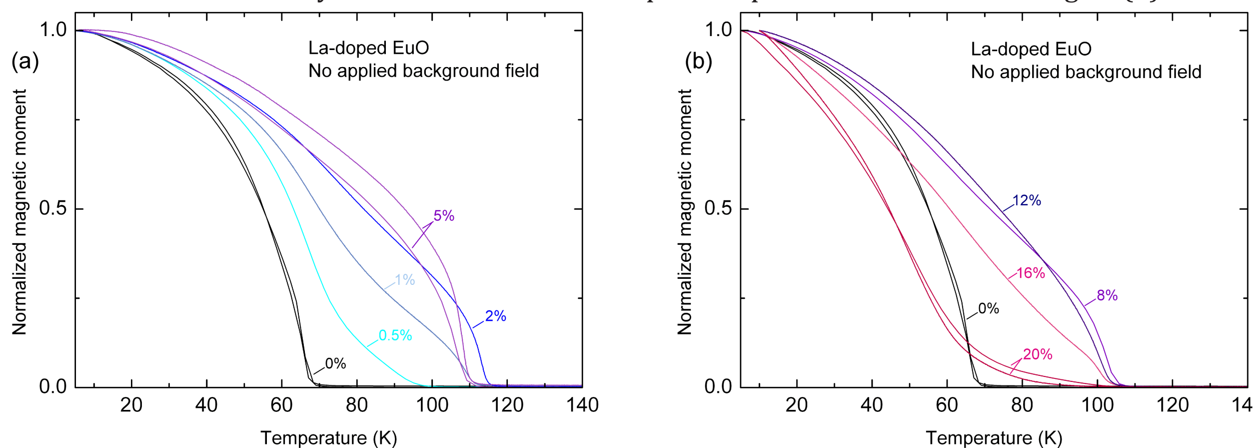

FIG. S10. (Color online) Normalized magnetic moment of $Eu_{1-x}La_xO$ films deposited at 275 °C on $YAlO_3$ substrates as a function of temperature measured by SQUID magnetometry with no applied background field. (a) Graphs for La doping levels between 0 and 5% and (b) graphs for La doping levels between 0 and 20%.

The disturbance to the magnetic lattice caused by doping with nonmagnetic ions has a less pronounced effect on T_{FM} when measured in external magnetic fields. Therefore, the maximum in T_{FM} of Lu-doped samples is expected to shift to higher doping concentrations in higher external magnetic fields. This effect is observed. The maximum in T_{FM} of the Lu-doped EuO films grown at $T = 250$ °C shifts from 5% (Fig. S8(b)) to 8% doping (Fig. S9) as the background magnetic field, $\mu_0 H$,

is increased from 2.5 mT to 1 T. With this increase, T_{FM} goes from 126 K (5%) and 123 K (8%) to ~168 K (5%) and ~185 K (8%). We note that the T_{FM} with a 1 T applied background field for our 8% Lu doped sample grown at $T = 250$ °C is comparable to the T_{FM} of the 8% Lu-doped sample grown using adsorption-controlled conditions reported in [6]. Here it should also be noted that applying magnetic background fields not only shifts the onset of ferromagnetism to higher temperatures, but also reduces the slope of the $M(T)$ response characteristic. Changing the slope criterion in the determination of T_{FM} therefore can lead to large differences in T_{FM}, illustrating the difficulty of defining a FM ordering temperature for samples measured in elevated background fields.

We determined the saturation magnetization M_{Sat} of the Lu-doped EuO films grown at $T = 250$ °C from ferromagnetic hysteresis loops (Fig. S11). To extract the film magnetizations, we measured the $M(T)$ characteristic of a $LuAlO_3$ substrate and subtracted it from the total sample magnetization. At low doping concentrations, our films show M_{Sat} values close to the theoretical bulk value of EuO: 7 μ_B/Eu-atom [16]. At high x>5%, there is a clear reduction of M_{Sat} with increasing x, as expected in the case of doping with nonmagnetic ions such as lutetium. The relatively large error bar of M_{Sat} is caused by the uncertainty in the film thickness of ±10%, due to the possible degradation of the surface of the EuO film.

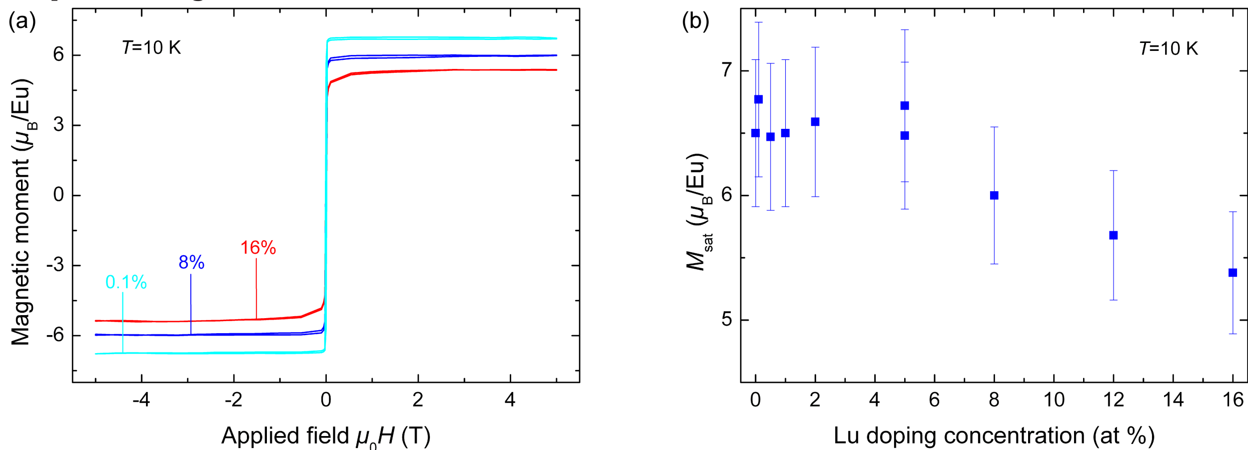

FIG. S11. (Color online) (a) Exemplary in-plane ferromagnetic hysteresis loops measured by VSM magnetometry for three different Lu-doped EuO films grown on $LuAlO_3$ substrates. The curves have been corrected for the signal of the bare substrates; (b) saturation magnetization M_{Sat} of $Eu_{1-x}Lu_xO$ films as a function of x determined from the magnetic hysteresis loops.

Determination of the Lanthanum Valence in La-doped EuO by STEM-EELS

The mechanical polishing techniques that typically are used for the preparation of conventional STEM-EELS specimens can be applied to EuO if water-free lubricants are used [17]. Alternatively, focused ion beam preparation has been shown to be successful in the preparation EuO specimens [17].

The 8% La-doped EuO film grown in the adsorption-controlled regime shown in Figs. 2(a)-2(d) was grown specifically for STEM-EELS investigations and consisted of a ~17 nm thick buffer layer of undoped EuO followed by ~17 nm of La-doped EuO. This sample geometry allowed us to compare variations in the europium occupancy of atomic-columns (expected as a dopant compensation mechanism in the La-doped part of the film) with that of the pure EuO film.

To investigate possible additional reasons for dopant deactivation in EuO, we measured the homogeneity of the valence of the lanthanum atoms in the 8% La-doped EuO film grown at low temperature; this is the same film characterized in Fig. 3. As can be seen in Fig. S12, the lanthanum valence is homogeneous across the La-doped EuO film including the region near the substrate, the over-oxidized La-doped EuO film near the capping layer, and the $LaAlO_3$ capping layer. Therefore, it can be assumed that all of the La-atoms in the La-doped EuO assume a 3+ valence, ruling out a possible 2+ lanthanum valence as a reason for the incomplete dopant activation of the La-doped EuO films.

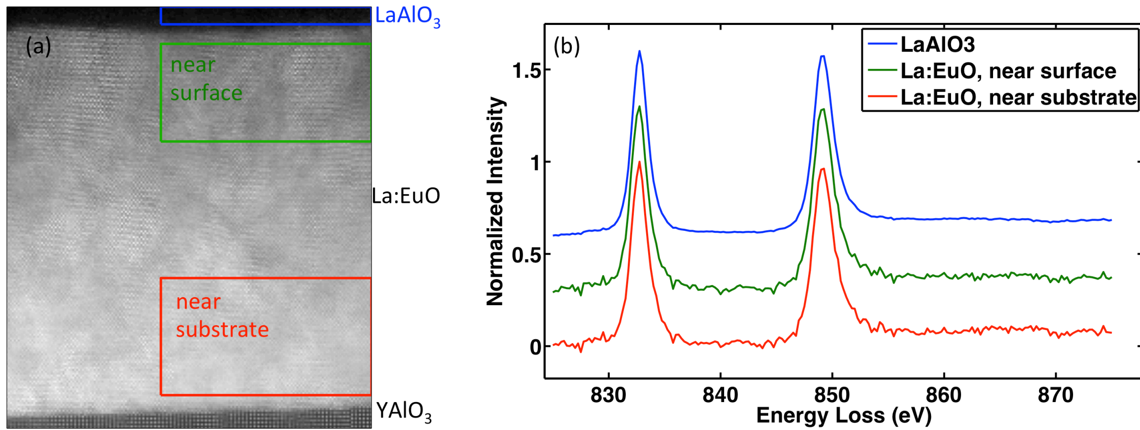

FIG. S12. (Color online) (a) Simultaneous ADF from data in Fig. 3 of the 8% La-doped EuO film grown at low temperature. (b) La-$M_{4,5}$ edge of the $LaAlO_3$ capping layer, the La doped EuO near the top surface of the film, and near the bottom of the film close to the substrate. The similar La-$M_{4,5}$ edges indicate that the lanthanum valence stays the same across the different regions (nominally 3+).

References

[1] D. V. Averyanov, O. E. Parfenov, A. M. Tokmachev, I. A. Karateev, O. A. Kondratev, A. N. Taldenkov, M. S. Platunov, F. Wilhelm, A. Rogalev, and V. G. Storchak, Nanotechnol. **29**, 195706 (2018).

[2] V.N. Abramov and A. I. Kuznetsov, Fiz. Tverd. Tela (Leningrad) **20**, 689 (1978).

[3] V. Kolobanov, V. Mikhailin, N. Petrovnin, D. Spassky, Y. Zorenko, Phys. Status Solidi B **243**, R60 (2006).

[4] A. Melville, T. Mairoser, A. Schmehl, T. Birol, T. Heeg, B. Holländer, J. Schubert, C. F. Fennie, and D. G. Schlom, Appl. Phys. Lett. **102**, 062404 (2013).

[5] A. Schmehl, V. Vaithyanathan, A. Herrnberger, S. Thiel, C. Richter, M. Liberati, T. Heeg, M. Röckerath, L. F. Kourkoutis, S. Mühlbauer, P. Böni, D. A. Muller, Y. Barash, J. Schubert, Y. Idzerda, J. Mannhart, and D. G. Schlom, Nat. Mater. **6**, 882 (2007).

[6] T. Mairoser, F. Loder, A. Melville, D. G. Schlom, and A. Schmehl, Phys. Rev. B **87**, 014416 (2013).

[7] A. Melville, T. Mairoser, A. Schmehl, D. E. Shai, E. J. Monkman, J. W. Harter, T. Heeg, B. Holländer, J. Schubert, K. M. Shen, J. Mannhart, and D. G. Schlom, Appl. Phys. Lett. **100**, 222101 (2012).

[8] N. J. C. Ingle and I. S. Elfimov, Phys. Rev. B **77**, 121202 (2008).

[9] T. Mairoser, A. Schmehl, A. Melville, T. Heeg, L. Canella, P. Böni, W. Zander, J. Schubert, D. E. Shai, E. J. Monkman, K. M. Shen, D. G. Schlom, and J. Mannhart, Phys. Rev. Lett. **105**, 257206 (2010).

[10] M. Matsubara, A. Schmehl, J. Mannhart, D. G. Schlom, and M. Fiebig, Phys. Rev. B **81**, 214447 (2010).

[11] A. Mauger, M. Escorne, C. Godart, J. P. Desfours, and J. C. Achard, J. Phys. Colloq. **41**, C5 (1980).

[12] T. Matsumoto, K. Yamaguchi, M. Yuri, K. Kawaguchi, N. Koshizaki, and Koji Yamada, J. Phys.: Cond. Mat. **16**, 6017 (2004).

[13] R. Sutarto, S. G. Altendorf, B. Coloru, M. Moretti Sala, T. Haupricht, C. F. Chang, Z. Hu, C. Schüßler-Langeheine, N. Hollmann, H. Kierspel, J. A. Mydosh, H. H. Hsieh, H.-J. Lin, C. T. Chen, and L. H. Tjeng, Phys. Rev. B **80**, 085308 (2009).

[14] S. G. Altendorf, A. Reisner, C. F. Chang, N. Hollmann, A. D. Rata, and L. H. Tjeng., Appl. Phys. Lett. **104**, 052403 (2014).

[15] S. G. Altendorf, A. Efimenko, V. Oliana, H. Kierspel, A. D. Rata, and L. H. Tjeng, Phys. Rev. B **84**, 155442 (2011).

[16] B. T. Matthias, R. M. Bozorth, and J. H. Van Vleck, Phys. Rev. Lett. **7**, 160 (1961).

[17] J. A. Mundy, D. Hodash, A. Melville, R. Held, T. Mairoser, D. A. Muller, L. Fitting Kourkoutis, A. Schmehl, and D. G. Schlom, Appl. Phys. Lett. **104,** 091601 (2014).